Fermilab

Fermilab Italian Students Program
Final report

DUNE ND-LAr 2x2 Demonstrator Tests

Vanessa Cerrone

Supervisors: Prof. Antonio Ereditato, Ting Miao
Co-supervisor: Geoff Savage

Abstract
A modular liquid argon (LAr) Time Projection Chamber (TPC) will be part of the near-detector facility for the Deep Underground Neutrino Experiment (DUNE) [1]. Such a TPC is being developed by the ArgonCube collaboration [2]. To demonstrate the feasibility of the LAr DUNE Near Detector, a medium size prototype has been built: the ArgonCube 2x2 Demonstrator. The detector will be placed in the MINOS-ND hall, upstream of the current MINERνA/MINOS-ND locations, at Fermilab. Currently two modules are being tested at the Liquid Argon Test Facility (LArTF), before being place on-axis in the NuMI neutrino beam.
The present report will be focused on the work done within the 2x2 Demonstrator group: the first part of the project is focused on the Low Noise AC Power distribution at LArTF, whereas the second is related to the 2x2 demonstrator light readout system tests.

Keywords
Neutrinos — LArTPC — Electronics

Contents

1. Introduction

DUNE is a next-generation accelerator neutrino oscillation experiment [1]. DUNE will utilize an intense beam of predominantly muon (anti)neutrinos produced at Fermilab, will sample the unoscillated beam on the Fermilab site, 574m from the proton target and 62 m underground, and then will sample the oscillated beam 1300 km away and 1.5 km underground, at the Sanford Underground Research Facility (SURF) in South Dakota, using four 10 kt liquid argon (LAr) target modules. By using LAr time projection chambers (TPCs), DUNE benefits from the exquisite precision to look at the particles escaping the nucleus, and measuring the neutrino energies with unparalleled accuracy. An extensive research and development (R&D) program is currently ongoing to deliver detectors capable of fulfilling DUNE's physics goals. The unprecedented size of the DUNE far detectors (FDs) has motivated large-scale LArTPC tests, in the single-and dual-phase ProtoDUNE modules in CERN, in themselves, the largest LArTPCs built to date. As the DUNE FDs have LAr targets, there will also be a major LAr component for the DUNE near detector (ND) suite, in order to minimize cross section and detector systematic uncertainties for oscillation analyses. However, the intense neutrino flux and high event rate at the ND makes traditional, monolithic, projective wire readout TPCs unsuitable, which has motivated a program of R&D into a new LArTPC approach, suitable for such a high rate environment, known as ArgonCube [4].

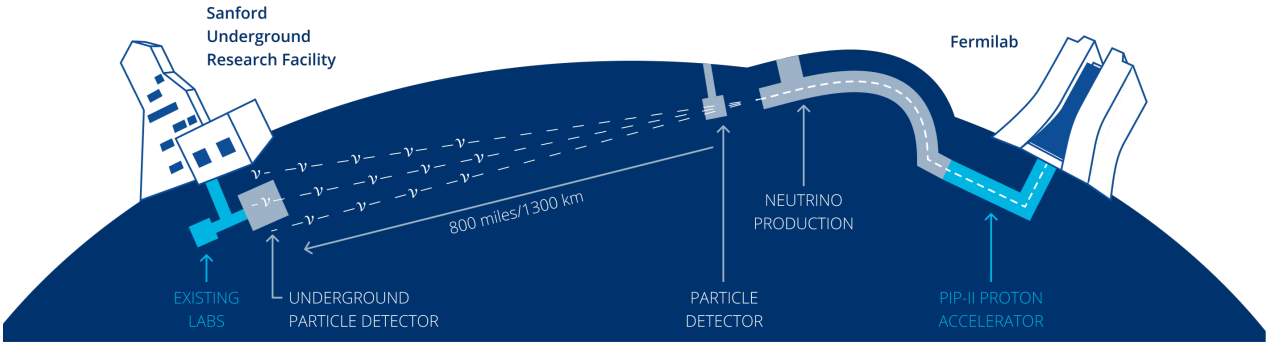

Figure 1. Cartoon illustrating the configuration of the LBNF beamline at Fermilab, in Illinois, and the DUNE detectors in Illinois and South Dakota, separated by 1300 km.

1.1 Physics goals

The scientific goals of DUNE are described in detail in [1]. The driving goals are to:

- Conduct a comprehensive program of neutrino oscillation measurements using the intense LBNF (anti)neutrino beam;
- Search for proton decay in several decay modes;
- Detect and measure the ν_e flux from a core-collapse supernova within our galaxy, should one happen during the lifetime of the experiment.

A rich program of ancillary science goals is enabled by the powerful LBNF beam and the detectors that will comprise DUNE. These include:

- Other accelerator-based neutrino flavor transition measurements with sensitivity to BSM phenomena;
- Measurements of neutrino oscillations using atmospheric neutrinos;
- Searches for dark matter;
- A rich program of neutrino interaction physics, including a wide range of measurements of neutrino cross sections and studies of nuclear effects.

1.2 DUNE Near Detector

The Near detector facility [3], depicted in Figure 2, comprises three components:

- The first component is a Liquid Argon TPC (LArTPC) constructed using the ArgonCube technology [4]. This component detector of the DUNE ND is called ND-LAr. This detector has the same target nucleus and uses the same fundamental detection principles as the FD. In-depth details about the usage of LArTPC in the DUNE ND will be provided in Section 2.
- The ND-GAr detector (also sometimes called the multipurpose detector, or MPD) consists of a high pressure gaseous argon TPC surrounded by an electromagnetic calorimeter (ECAL) in a 0.5 T magnetic field with a muon system outside of that. Since ND-GAr can access lower-momentum protons than ND-LAr and has superior identification of charged pions, events occurring in ND-GAr will be valuable for studying the charged particle activity near the interaction vertex. ND-LAr and ND-GAr can move to take data in positions off the beam axis. This capability is referred to as the DUNE Precision Reaction-Independent Spectrum Measurement (DUNE-PRISM).
- The final component of the DUNE ND suite is a magnetized beam monitor called the System for on-Axis Neutrino Detection (SAND). This device monitors the flux of neutrinos going to the FD from an on-axis position where it is much more sensitive to variations in the neutrino beam. SAND consists of an inner tracker surrounded by an ECAL inside a large solenoidal magnet.

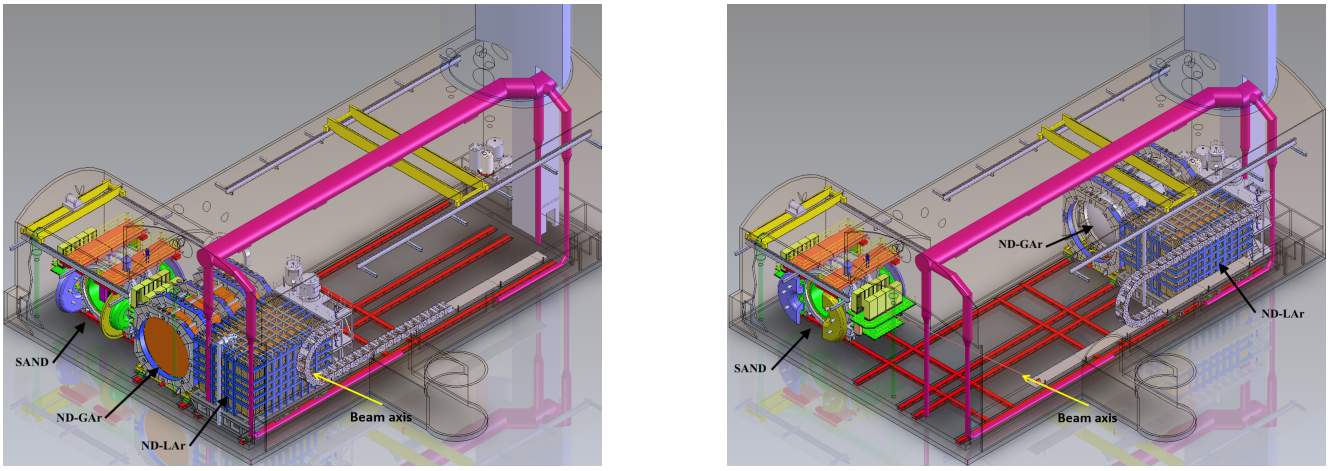

Figure 2. Schematic of the DUNE ND hall shown with component detectors all in the on-axis con- figuration (left) and with the ND-LAr and ND-GAr in an off-axis configuration (right). The SAND detector is shown in position on the beam axis. The beam axis and direction is indicated.

The following few sections will mainly focus on the ND-LAr component since this is the most relevant in the scope of this internship project.

2. LArTPC in the DUNE ND

This section is aimed at providing a brief description of traditional LArTPC detectors and then introduce the ArgonCube concepts and ideas for an innovative design for LArTPCs.

2.1 Working Principle of a LArTPC

A TPC is a detector technology enabling a 3D track reconstruction of charged particles passing through the active detector material, which, in the case of a LArTPC [5, 6], is liquefied argon. The basic working principle of a TPC is

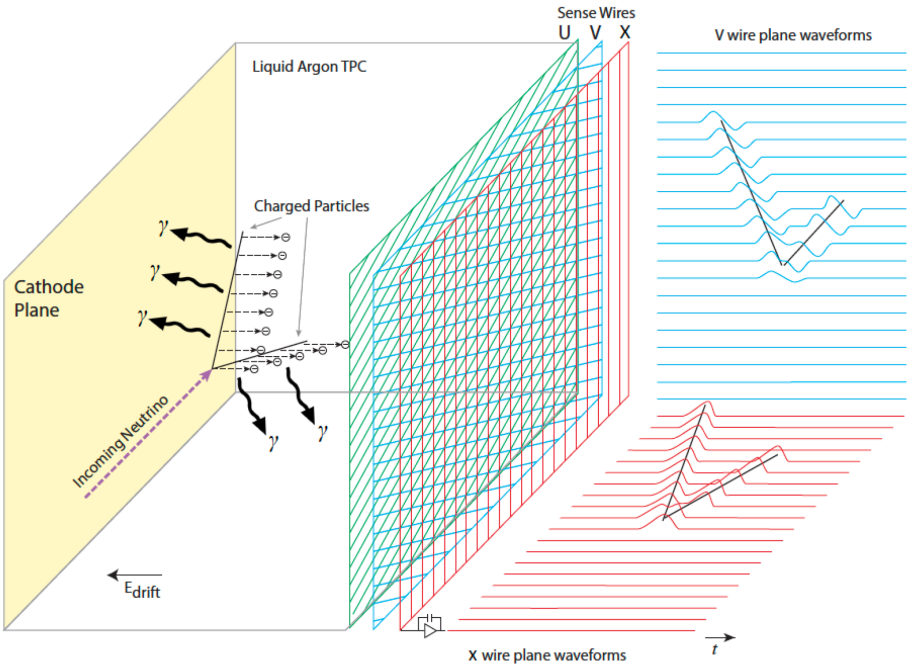

Figure 3. Working principle of a traditional TPC (scheme from [7]). Ionization electrons and the ionized atoms drift to the anode and the cathode, respectively. At the anode plane, a charge readout system detects the charge. The first two wire planes (U and V) are operated at a small positive bias voltage so that the electrons are able to traverse the planes in between the wires and eventually be collected at the X plane. The U and V planes only record an induction signal, whereas the X plane sees the actual signal produced by the collected charge.

illustrated in Figure 3. Neutrinos charged current (CC) interactions with the LAr target produce either muons or electrons, depending on the neutrino flavor. These charged particles interact with argon atoms, exciting or ionizing them. Consequently, scintillation light and ionization electrons are abundantly produced. Due to the electric field applied between the anode and the cathode, the free electrons drift towards the anode, where they are detected by a charge readout plane (conventionally projective wire readouts). The detection of the prompt scintillation light (to which LAr is highly transparent) with a light readout system can be used for the determination of the time of the interaction. Combining the 2D spatial information of the charge readout with the time signal of the scintillation light and the knowledge of the electron drift velocity allows for a 3D reconstruction of event vertices and particle tracks.

2.2 ArgonCube technology

Traditional monolithic LArTPCs with drift fields of the order of 100 Vcm^{-1} and drift distances of several meters require high cathode bias voltages ($\sim$ 100 kV): the large amount of energy stored in the TPC poses severe risks in case of an electric breakdown. To address this issue, the ArgonCube collaboration [4] developed an innovative project for LArTPCs, i.e. a modular design, where several identical LArTPC modules are combined together to make up a large detector.

The ArgonCube technology has introduced a wide range of innovations [8, 9]:

- **Modularization**: main characteristic of the ArgonCube concept. As previously mentioned, each module is a self-contained TPC, electrically isolated from the others. A central cathode splits each TPC into two optically isolated drift regions. In this way, the drift length is naturally reduced. Shorter drift paths allow the system to be operated at smaller cathode bias voltages, leading to a reduced amount of stored electric field energy at the same drift field intensity; it also reduces the LAr purity requirements, since the charge and light signals are

less attenuated with respect to a monolithic larger TPC[1] [10].

- **Pixelated charge readout**: a novel pixelated charge readout enables full 3D tracking capabilities and tackles the event pile-up problem due to the high rate environment in which the ND is expected to work. Further information can be found in [11].

- **Light readout**: the ArgonCube collaboration developed two complementary light detection systems [12] using Silicon Photomultipliers (SiPM) coupled to dielectric structures, which can be used within high strength electromagnetic fields. This eliminates additional dead volume, traditionally needed in PMT-based light readouts. Since the part of the internship work was focused on testing the light readout system, additional details about it will be provided in Section 4.

2.3 ND-LAr 2x2 demonstrator

The ND-LAr detector design can be found in [3]: it will consist of 35 ArgonCube modules, grouped into 7 rows of 5 modules, submerged in a common bath of purified LAr.
After successfully testing small-scale TPCs [14], the next step in the ArgonCube program is to demonstrate the scalability (to large active masses) of the charge and light readout systems, and to show that information from separate modules can be combined to achieve high quality event reconstruction [13]. To that end, a mid-scale modular TPC, called ArgonCube 2x2 Demonstrator has been designed. This demonstrator consists of four LArTPC modules arranged in a 2x2 grid within a shared high-purity LAr bath (see Figure 4). Each TPC module has a footprint of 0.7 m by 0.7 m, and is roughly 1.4 m tall. Each module features a relatively short drift length and a fully independent TPC with its own charge readout, light detection system and cryogenics.

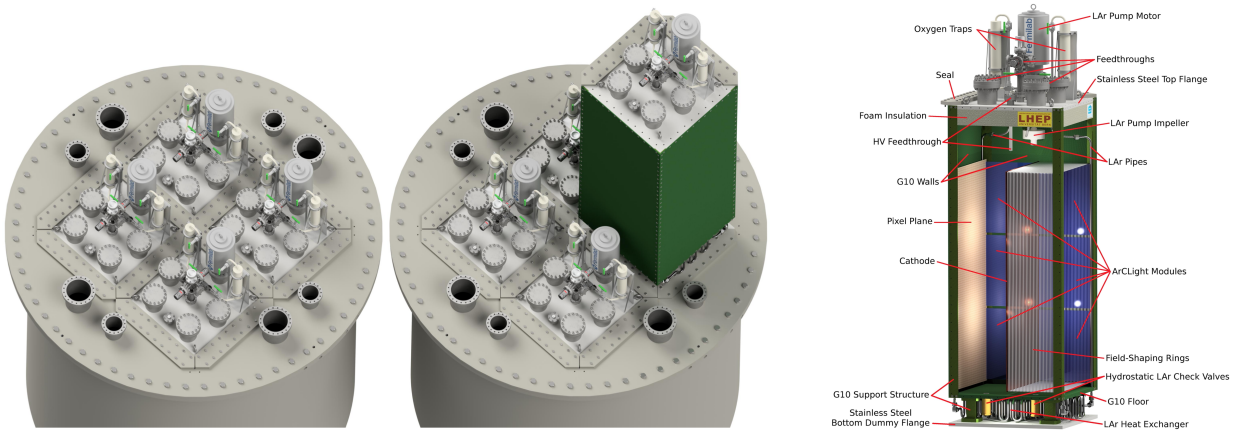

Figure 4. LEFT: Illustration of the ArgonCube 2x2 Demonstrator module. The four modules are visible, and one of them is partly extracted. RIGHT: Cutaway drawing of an ArgonCube module for the 2x2 Demonstrator. Figures were taken from [13].

All 4 modules will be assembled as a prototype modular detector in MINOS hall and operated in the neutrinos from the main injector (NuMI) on-axis beamline [13]. Hence, it will be the first DUNE detector to take neutrino events, thereby providing the first neutrino beam run with comparable few GeV intensity. ArgonCube 2x2 will then be operated underground at MINOS hall, where scintillator planes repurposed from the MINERνA experiment will be placed upstream and downstream of the ArgonCube 2x2 (in the so-called ProtoDUNE-ND) to provide upstream and downstream tracking. A scheme of the experimental hall is reported in Figure 5.

[1] For example, electro-negative impurities (e.g., water, oxygen, and nitrogen) attenuate signals and can cause scintillation light quenching. Moreover, the scintillation light is affected less by Rayleigh scattering, i.e. photons scattering off particles smaller than the photon wavelength.

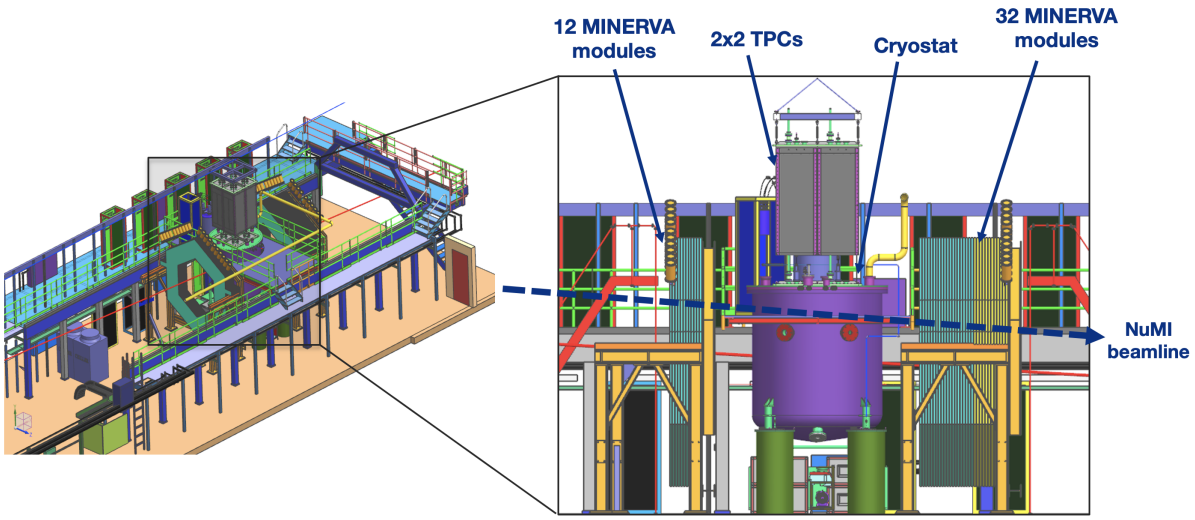

Figure 5. ProtoDUNE-ND in MINOS hall. The few GeV intense neutrino beam from NuMI is incident from the left. Scintillators plates from the MINERνA experiment will be located upstream and downstream of the ArgonCube 2x2 Demonstrator. Schemes from T. Miao (FNAL) .

3. LArTF 'Low Noise' AC Power Distribution

Before commissioning the system underground in MINOS hall ArgonCube 2x2 modules will be tested in the Liquid Argon Test Facility, at Fermilab. The neutrino interaction events which the DUNE Near liquid argon detector is designed to sense produce very low-level electrical signals that are easily overwhelmed by typical earth grounding system electrical fluctuations, or noise. To insure adequate sensitivity of the detector and minimize noise transmission, a special ground system is put in place to isolate the detector electronics and instrumentation from all other electrical systems, equipment and metallic components connected to the building ground scheme. All of the components of detectors are referenced at a single isolated node, so we refer to it as **single-point grounding configuration**.

3.1 Ground system at LArTF

To support ArgonCube TPC operations, the Low Noise AC Power Distribution system to power the 2×2 modules has been upgraded at the Liquid Argon Test Facility (LArTF) [15]. The upgrade includes the latest design of the Impedance Monitor system including a custom designed, commercially built, saturable inductor (SI) and Ground Current Impedance Monitor (GIZMo). The system monitors the integrity of the single ground and provides an audible and visual alarm if a rogue short (connection) exists in the system (i.e. other connections made to ground besides the safety ground).

3.2 Impedance monitor overview

Its main constituents are:

- **Zedboard**: it features a Zynq chip, i.e. a "System-on-Chip" that combines an FPGA and a dual-core ARM processor (XC7Z020);
- **Lock-in-amplifier**: it is used to detect and measure very small AC signals, even in presence of significant noise sources. Thanks to the phase-sensitive detection technique, it is able to single out the component of the signal at a specific reference frequency and phase. Noise signals, at frequencies other than the reference frequency, are rejected and do not affect the measurement;

- **LED display**: the front panel display in Figure 6 has a large numerical value which corresponds to the systems estimate of the resistance between the detector ground and the building ground in ohms. It is mainly exploited for monitoring and debugging purposes;
- **Speaker and alert beacon**: audible and visual alarm are provided in case of a rogue short.

Figure 6. GIZMo front panel. The resistance numerical value is shown on the right-hand-side.

3.2.1 Working mechanism

A simplified version of the GIZMo circuit design is reported in Figure 7. The operation mechanism is based on the following steps [16]:

- A small AC current is injected into the detector through the Digital-to-Analog Converter (DAC). Currently, the excitation waveform is a sine wave with an amplitude of approximately 22 mA and a frequency of 1.4 kHz;
- When no other connections to building ground exist, this current will return in its entirety through the safety ground wire back to building ground;
- The safety ground wire passes through a current transformer, used to measure the current flowing through the saturable inductor while providing minimum disturbance to the circuit itself;
- The saturable inductor is used for safety issues: indeed, in case of any fault, accumulation of charge might cause the potential of reference node to rise above the safety level, which poses a shock hazard.

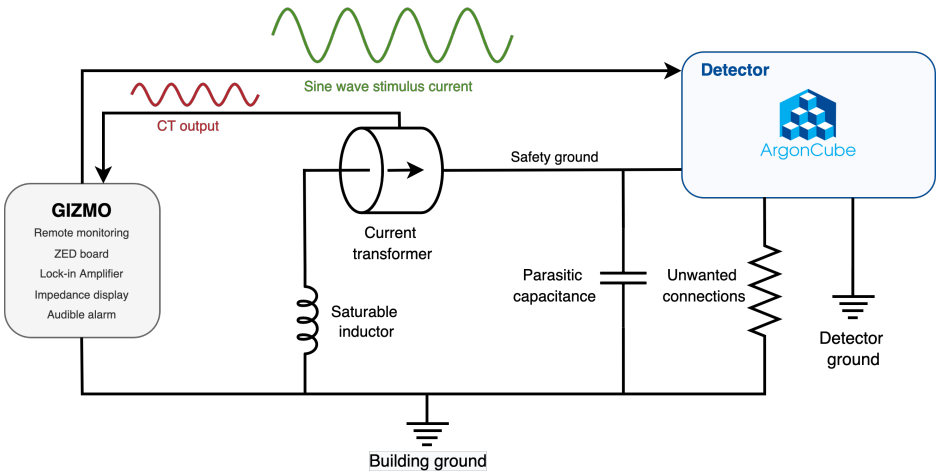

Figure 7. Simplified scheme of GIZMo circuit.

3.3 Impedance Monitor characterization measurement

We model the circuit as a fixed impedance (Z) (composed of the saturable inductor and the parasitic capacitance of the detector) in parallel with a potential short between detector ground and building ground (R). Since the excitation current is fixed, we measure the amplitude of the digitized waveform as:

$$V = \frac{Z \cdot R}{Z + R} \cdot I \tag{1}$$

To determine the capacitive coupling to the building or resistive short magnitude of the experiment, one needs a characterization curve of the system, prior to releasing the system to operations. Thus, resistive and capacitive decade boxes can be used to evaluate the response of the system.
At first all detector ground connections are disconnected from the cryostat. In this configuration, a resistive decade box is connected between the detector ground wire and a building ground reference. The resistance is increased until the display value returns to the initial condition (for an open circuit, hence detector ground disconnected from the cryostat). The data points resulting from this procedure are shown in Figure 8: an interpolation was performed to obtain the calibration parameters to extract the impedance between the detector and building grounds as a function of the variable resistance. The measured baseline without capacitive or resistive load was roughly 152 Ω and from the fit results we can infer that the values stabilizes around 142 Ω.

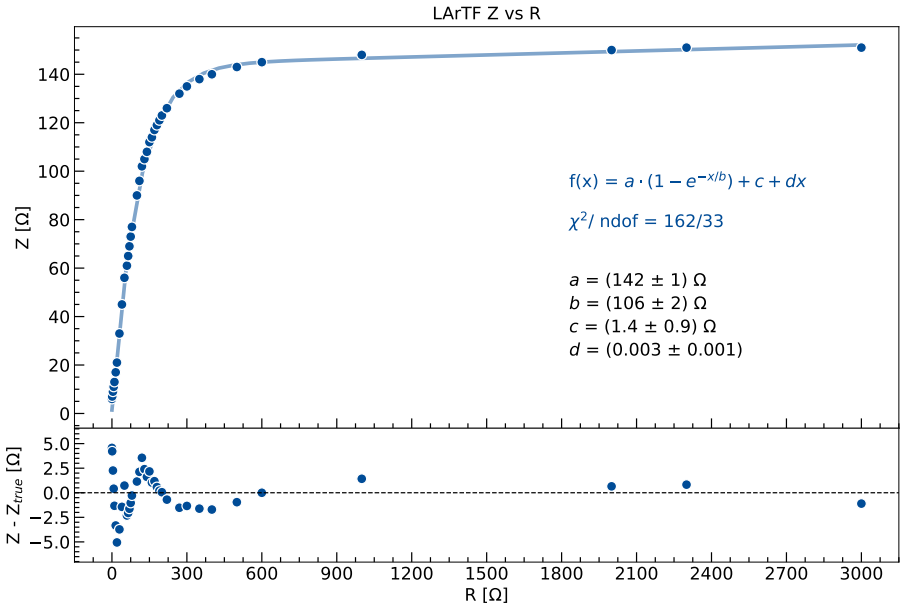

Figure 8. Measured impedance detector-building grounds as a function of variable resistance. The best fit function and the obtained parameters are also indicated.

The detector ground cable is then connected to the 2x2 module-1[2] and similarly the capacitive decade box wires are connected between the detector ground lead and a building ground reference. When the capacitance is 0 nF the displayed value should be the same as the initial value. The capacitance is then increased in steps of 2-3 nF. To estimate the capacitive coupling, an interpolation of C as a function of Z is carried out. The results for two possible cases are reported in Figure 9.

[2]Module-1 was being tested at that moment.

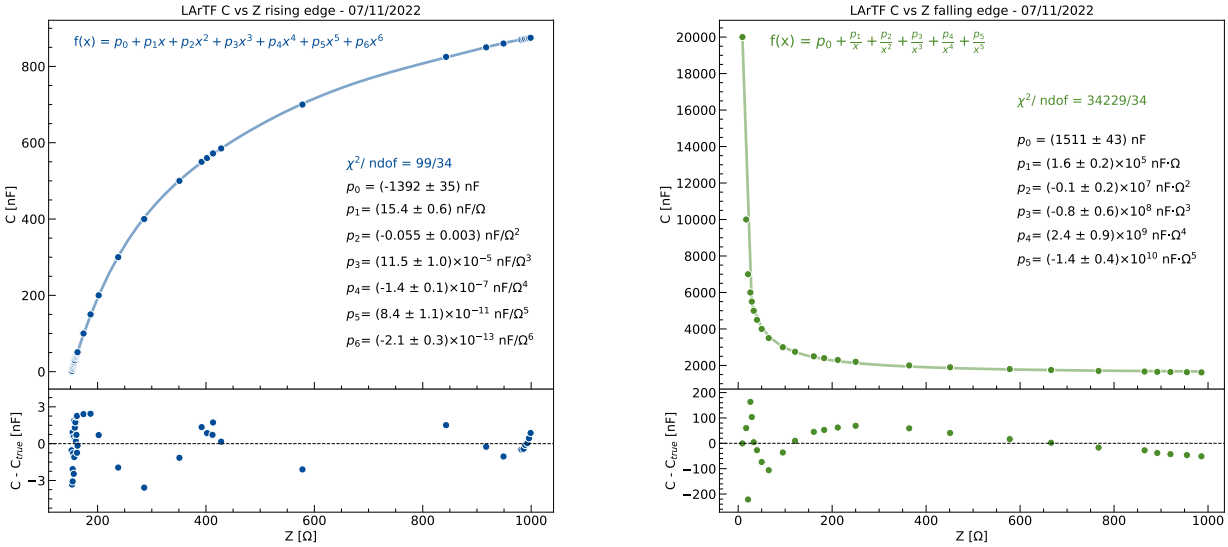

Figure 9. Measured impedance as a function of different capacitance values. LEFT: characteristic curve for a system on the rising edge of the curve. RIGHT: characteristic curve for a system on the falling edge of the curve.

There are three possibilities:

- If the impedance increases, the system is on the rising edge of the curve, as shown in Figure 9 on the right-hand-side.
- If the impedance decreases, the system is on the falling edge of the curve (see left panel of Figure 9).
- If the display indicates a smaller value than the baseline, the cryostat has a conductive connection to the building ground, which should be removed before releasing the system to operations.

2x2 Module-1 was on the rising edge C curve and the measured impedance was of the order of 160 Ω when connected. Using the fit parameters (displayed on the left panel of Figure 9), we can retrieve the capacitive coupling, which turns out to be ~ 38 nF.

3.4 GIZMo slow control

GIZMo identifies shorts between building and detector ground, and it is crucial to be able to monitor how the impedance value changes throughout time. My task consisted in developing a procedure to do so[3]. Thanks to the internal architecture of the monitor, it is possible to have remote access via SSH connection. Firstly, an ssh connection to GIZMo is established through one of the servers. Then, the readout program is launched: `GIZMO.elf` reads the hardware and prints values in the shell. The python script loops and reads the values via the shell. They are finally temporarily stored. Even though the quantity of interest is the impedance, the program also provides other parameters, i.e., charge, current, amplitude and set threshold. All of them are stored in **InfluxDB** [17], an open-source time series database. For this purpose, the InfluxDB-python library is used, acting as a Python client interacting with InfluxDB. Finally, live monitoring is implemented through **Grafana** [18], an open source analytics and interactive visualization web application, that allows to visualize all the previously mentioned parameters.

[3]The scripts can be found at the following link: https://github.com/vanessacerrone/gizmo_control

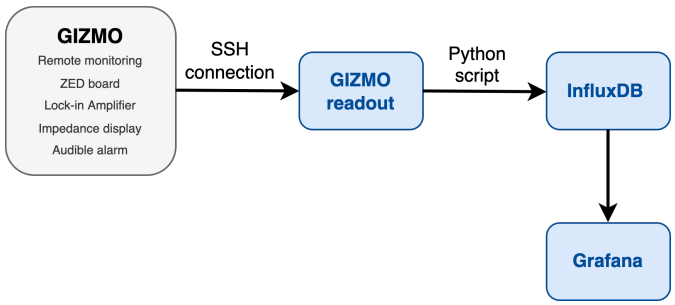

Figure 10. Simplified schematics of connections to implement live monitoring of GIZMo.

A simplified scheme of the connections, from the impedance monitor to Grafana, is reported in Figure 10.

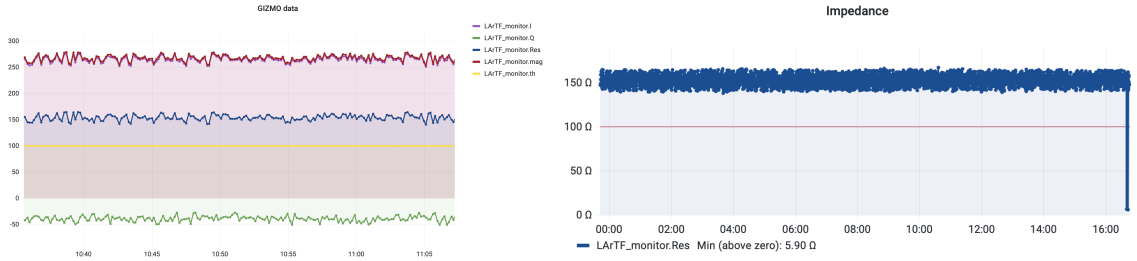

Figure 11. Example of Grafana dashboard. Left: current (purple), charge (green), resistance (blue), amplitude (red), threshold (yellow). Right: resistance value throughout time, with the fixed threshold highlighted. It is also possible to observe a sudden resistance drop in the right tail of the plot.

On the left panel of Figure 11, an example of the Grafana dashboard is reported: all the stored parameters are shown and can be visualized in real time. The right plot shows only the measured impedance between detector and building grounds; the red line represents the set threshold (100 Ω in this case): if the impedance acquires a lower value the audible alarm goes off to identify a possible short. Moreover, a python script was developed to automatically produce a summary plot every 24 hours, like the one in Figure 12.

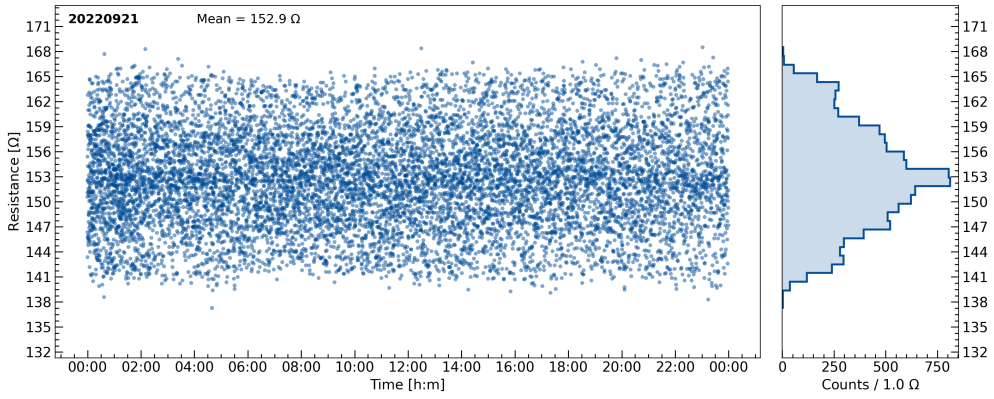

Figure 12. Summary plot of the measured impedance between detector and building grounds every 24 hours.

4. ArgonCube 2x2 Light Readout System (LRS)

The ArgonCube collaboration designed two complementary light detection systems using Silicon Photomultipliers (SiPMs) optically coupled to dielectric materials that can be employed within electric fields and sharing the same readout electronics: the ArgonCube Light readout system (ArCLight - ACL), developed at the University of Bern [12] and the Light Collection Module (LCM), developed at Joint Institute for Nuclear Research (JINR) in Dubna [19].

4.1 Scintillation light in LAr

Scintillation light is emitted by previously ionized atoms that recombine with electrons or excited atoms. In LAr the active mechanisms emit Vacuum Ultraviolet (VUV) photons, with a wavelength peaked around 128 nm. Most photon detection sensor have low quantum efficiency to detect VUV light (VUV-optimized photo-sensors reach at most 15% [20]). Therefore, many experiments use a wavelength shifter (WLS), i.e. a material that is able to absorb the VUV light and isotropically re-emit it at a longer wavelength (e.g., optical blue). Both Light Readout Systems (LRS) employed in the 2x2 Demonstrator are based on this principle.

4.2 LRS overview

As previously mentioned, two light systems are employed:

- The ArCLight readout systems was developed at LHEP[4] (Bern) [12]. It consists of a dielectric WLS bulk structure. A dichroic mirror foil coated with a thin layer of 1,1,4,4-Tetra-Phenyl-1,3-Butadiene (TPB) is attached on one side of the bulk structure. The TBS shifts VUV scintillation light to blue light, for which the dichroic mirror has a large transparency. Within the bulk, the blue light is shifted by the WLS to green light, which is efficiently reflected by the dichroic mirror. On all the other sides specular mirrors reflect the green light, making the module a light trap. This light is finally detected by SiPMs. One of the key features of this LRS is the accurate scintillation position reconstruction. Figure 13 shows the operation principle of an ACL module.
- The LCM module was mainly developed at the JINR[5], in Dubna [19]. It consists of a bundle of dielectric WLS fibers. The working principle is more or less the same as ACL modules: the VUV scintillation light is converted to blue light by a layer of TPB, the latter is eventually is shifted to green light inside the fiber, where it is trapped due to the fiber high efficiency for total internal reflection. Since both ends of the bundle of fibers are connected to a pair of SiPMs, the spatial resolution of the LCM is limited to the panel size. On the other hand, LCM modules are characterized by a high collection efficiency. Figure 14 shows the operation principle of a LCM module.

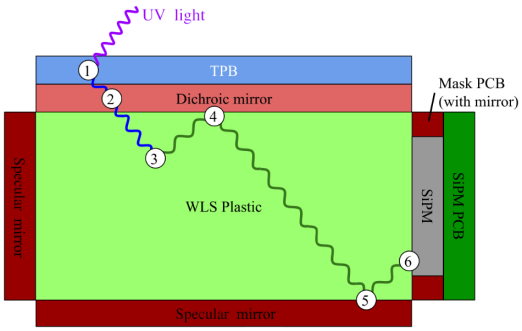

Figure 13. Schematic drawing illustrating the working principle of an ArCLight module. The figure was taken from [8].

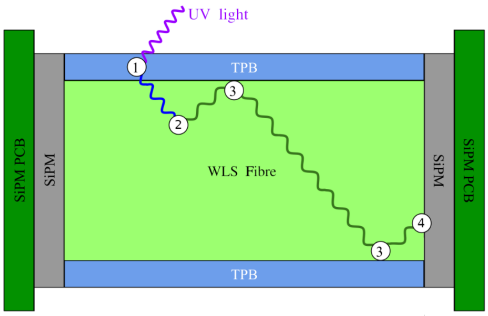

Figure 14. Schematic drawing illustrating the working principle of a LCM module. The figure was taken from [8].

[4]The Laboratory for High Energy Physics (LHEP), https://www.lhep.unibe.ch
[5]http://www.jinr.ru/main-en/

Each 2x2 prototype Module hosts 8 ArCLight tiles (surface dimensions 30 cm × 28 cm) and 24 LCM tiles (surface dimensions 10 cm × 28 cm). Each two SiPMs are mounted on a Printed Circuit Board (PCB). Each PCB has 2 double-pin connectors to plug it onto an E-shaped readout PCB (the so called E-PCB or E-board), which can support either 3 LCMs or 1 ArCLight module. Therefore, in both cases we have six SiPMs per ACL module or six SiPMs per LCM array. A simplified scheme of the two modules with the connections to the SiPMs is reported in Figure 15.

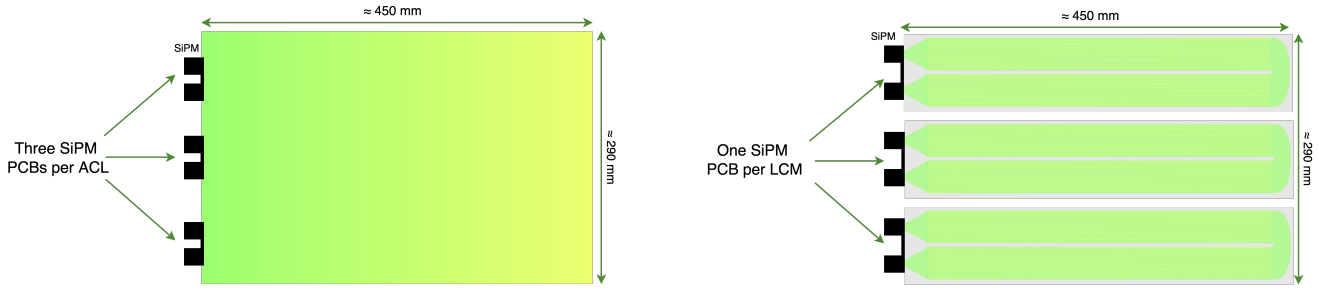

Figure 15. Schematic drawing of an ArCLight tile (left) and of a LCM array (composed of three LCM tiles).

4.3 LRS readout electronics

A scheme of the LRS readout electronics, only with the main components (needed for the scope of the tests presented in following sections) is given Figure 16. The Light Readout System (LRS) consists of 96 SiPMs and cold amplifiers which are inside the TPC module, hence the detector. The Front-End and Data Acquisition (DAQ) electronics are instead placed into two VME crates mounted onto separate racks, one hosting 4 Variable Gain Amplifiers (VGAs), each with 24 channels, the SiPM bias Power Supply (PS), and the control boards for both the VGAs and the SiPM bias voltage, while the second rack hosts 2 Analog-to-Digital Converters (ADCs).

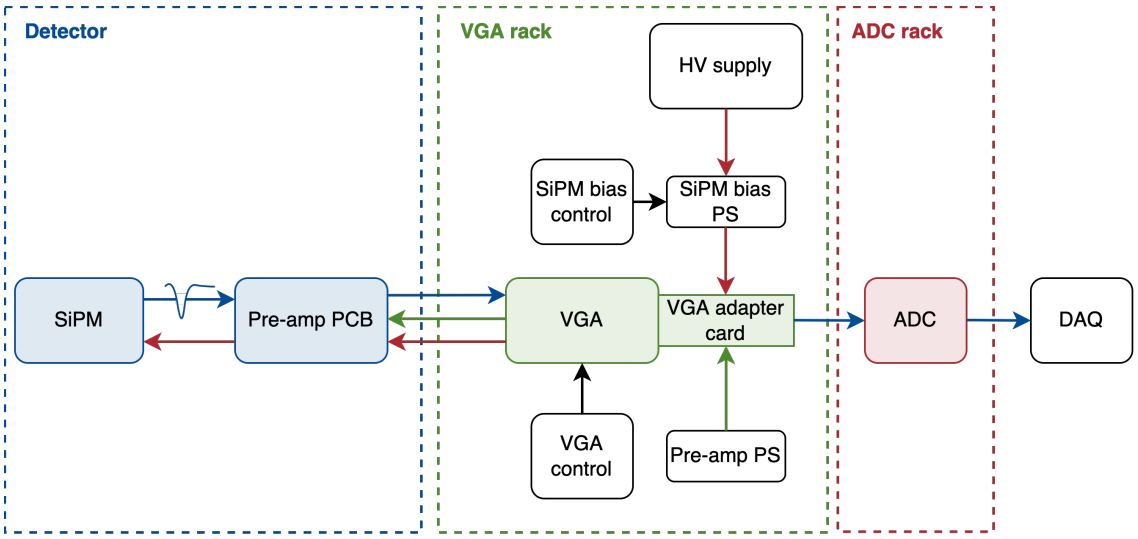

Figure 16. Scheme of the LRS readout electronics.

5. LRS QA/QC tests

A series of quality assurance/ quality control (QA/QC) tests are performed to validate the LRS functionality after transportation and to determine the overall electronics response and performance of the LRS. In this section, a first general summary of the tests is given, followed by details about each step.

The QA/QC testing of the light readout system electronics consists of three tests:

1. The first test is dedicated to check the integrity of the cable connections: in order to do so we check the current load on the low voltage DC power supply which powers the E-boards. With the VME crates powered up we can also verify communication with all readout electronics devices.

2. In the second step the full readout chain form SiPM to DAQ server is tested. Each device in the readout chain (VGA, ADC, SiPM bias supply) has to be powered up and configured. After following all the configuration steps, single p.e. noise should be visible for each channel on the ADC oscilloscope

3. In the last step of the LRS QA/QC the calibration LEDs are used to test the response of each single readout SiPM channel. Data runs at single photon regime are exploited to extract the SiPM gain. My work has been mainly focused on this final part.

The current setup at LArTF is shown in Figure 17.

Figure 17. Current setup at LArTF. Module-1, Module-0 and the two racks are visible.

5.1 Pre-tests

This pre-step is a not a test of the light detector itself but more of the electronics. It is dedicated to check the current load on low voltage (LV) DC power supply (PS) which powers the E-PCB of the LRS system. Cold pre-amplifiers built-in on the E-PCBs require ± 5 V/ 68 mA in warm (less in LAr), provided by the PS. Each module has 16 E-PCBs inside the cryostat (8 per TPC) and one VGA Adapter card distributes power to 4 E-PCBs. For the tests we used a PS with two output channels (± 5 V) supplying 4 VGA adapter cards with a 1:4 fan out cable. Thus, the current drawn through each adapter card is 68 mA $\times$ 4 = 272 mA (in warm). First of all we disconnect from the PS all the VGA adapter cards but one to test individual sets of 4 E-boards. If the drawn current is less than described above, it indicates problems either with the cable lines or connections or cold preamps on the E-PCBs. Finally we connect all the E-PCBs to the PS. In this configuration, the expected current draw is 68 mA $\times$ 16 = 1.088 A. This test verifies the integrity of the cable connections between the VGA adapter and the single E-boards. As next step both the VGA and ADC crates need to be powered up, making sure all power rails are on.

Results Module-1 was tested and all current draw measurements were consistent with expectations, thereby verifying the integrity of the cable connections.

5.2 Full chain testing

If the first step is successful, a test of the full LRS readout chain can be performed. First of all we establish communication to the VGA control board and then load the VGA configuration. Namely, we choose the VGA amplification, which can be from 0 to 24 dB. Each VGA has the same gain for all channels: for initial testing and calibration 24 dB is used, whereas for physics runs 6 dB is chosen. The same thing is carried out for the ADCs, establishing communication with them through the DAQ server and loading the proper configuration. Then the SiPM bias voltage has to be ramped up to ~ 90 V: before doing that it is crucial to make sure the module is sealed light tight. Turning on the SiPMs in ambient light could cause damage to them.
After following all the configuration steps, an external trigger is established via pulse generator and single photoelectron (PE) noise should be visible for each channel on the ADC oscilloscope. These PEs originate mostly from dark counts or residual ambient light. The expected noise rate at warm is $\mathcal{O}(1\,\text{MHz})$.

Results Module-1 LRS system was successfully tested and we did not find any more dead channels compared to the old runs that were performed in Bern before shipping the module to Fermilab.

5.3 LED calibration run

In the last step of the LRS QA/QC calibration LEDs are used to test the response of each SiPM channel. The LRS has four blue LED units inside (two per TPC) mounted on top and bottom of each TPC. To power the LEDs a pulse generator with the following settings is used:

- Frequency: 1 kHz
- Pulse width: 10 ns to 50 ns
- Amplitude: $\sim$20 V
- Rise time: as fast as possible
- Coupling: 50 Ω

As part of my work done related to this section, I developed a tool to perform calibration run analysis in a quick way during QA/QC tests: details will be given in Section 6.

6. LED calibration run analysis

As previously explained, during final QA/QC tests a LED calibration run will be performed. To this extent, data acquisition runs for each LED position with different amplitude settings are carried out, hence choosing which LED to trigger. In this way it is possible to extract the SiPMs gain factor by studying single PE spectrum. A dedicated software already exists, but it is sophisticated and takes order of hours to produce the results. A quick tool[6] to be used only during QA/QC tests becomes necessary to have an immediate feedback on channels that do not work properly.

6.1 SiPM charge spectrum

The analysis starting point is the SiPM charge spectrum, like the one shown on the left panel of Figure 18, obtained by integrating the signal waveforms in a specific time window (this is done by a dedicated software). Then I wrote a script that executes the following steps:

1. ROOT `TSpectrum` Class [21] is used to preliminarily search for peaks in the charge spectrum (the so called *finger plot*). One of the key parameters to manually set here is the threshold, namely peaks with amplitude less than threshold $\times$ amplitude of the highest peak are discarded.

[6] All the scripts I developed can be found here: https://github.com/vanessacerrone/2x2_LRS_tests

2. The peaks x-axis position is retrieved and used as an input parameter to perform gaussian fits. Each peak is separately fitted to extrapolate both the centroid and the standard deviation.

3. A linear interpolation is then carried out: specifically we fit the different peak distribution mean values as a function of the number of PEs. Therefore, from the slope of the curve we can extrapolate the single channel gain factor. An example for one single channel is reported on the right panel Figure 18.

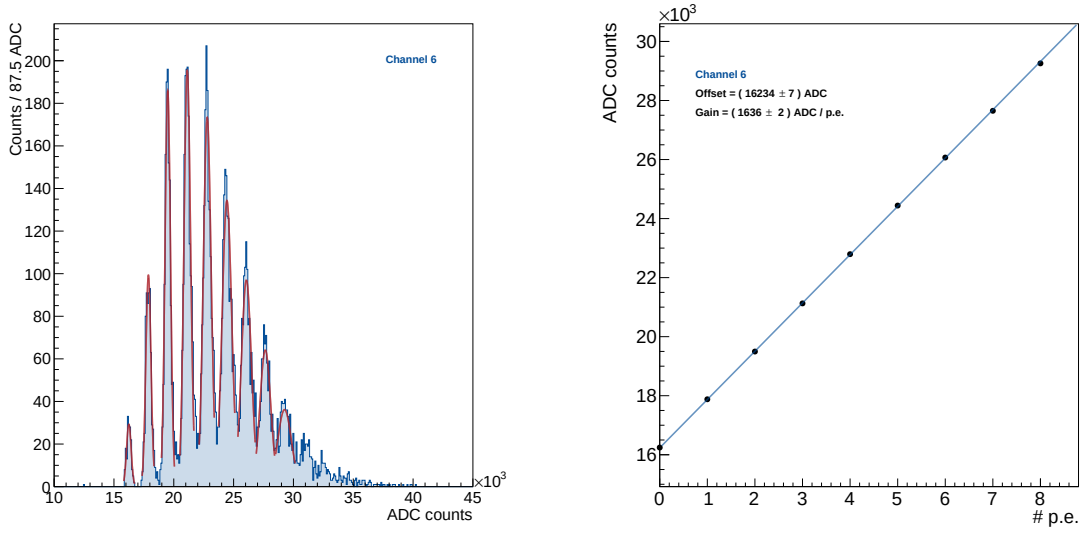

Figure 18. LEFT: SiPM charge spectrum. All peaks are fitted with a Gaussian function. RIGHT: Linear interpolation of the peaks mean value as a function of the number of PEs.

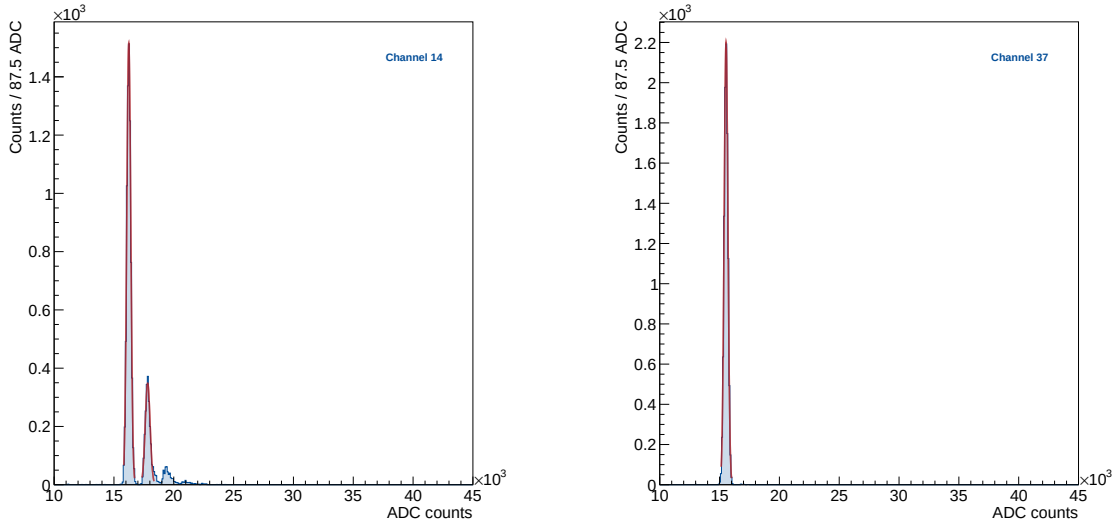

Figure 19. SiPM charge spectrum. All peaks are fitted with a Gaussian function. LEFT: this example is related to a light module that is far from the LED source; indeed a small number of PEs is detected. RIGHT: This spectrum corresponds to a module inside to the other TPC, hence not exposed the LED light.

Figure 18 (left) and Figure 19 show some examples of the charge spectra for a few of the 64 available ADC

channels. In this specific case we are looking only at ArCLight modules, and data was taken in cold in Bern. The light yield depends upon the position of the light modules with respect to the LED source. Indeed, we can see different output spectra: ADC channels connected to light modules which are close to the LED source will acquire a clean charge spectrum with several PE peaks (Figure 18 left). The farther ones are exposed to a smaller light yield so we expect to see higher noise and less photoelectrons (Figure 19 left). Data runs are acquired using as a trigger a single LED source, installed in one of the two TPCs, hence ADC channels connected to the other TPC will only record pedestal data (Figure 19 right). Moreover, some channels are inactive and will produce empty histograms, which are promptly discarded. The charge spectra for all the channels and for this specific data acquisition can be found in the Appendix; other data taken in cold (i.e. in LAr) in Bern, from both ACL and LCM, is available, but it is not shown in this report.

6.2 LED calibration run results

All channels data is processed[7] and the results are saved in a comma-separated-values (CSV) file containing channel number, number of peaks found and all the fit parameters. Then, another script takes this file as input and produces the plot reported in Figure 20: the latter shows the gain as a function of the channel number. We can observe three different patterns, which correspond to the aforementioned ones. The blue points represent what we call *valid channels*: in this case we have to verify whether the gain is in the expected range (which can be inferred from the individual run settings) and if it is more or less comparable among all channels (since each VGA has the same gain for all channels). For *inactive channels* the gain is set to 0 ADC/PE, whereas when only the pedestal is found, the gain is set to -1000 ADC/PE for graphical reasons.

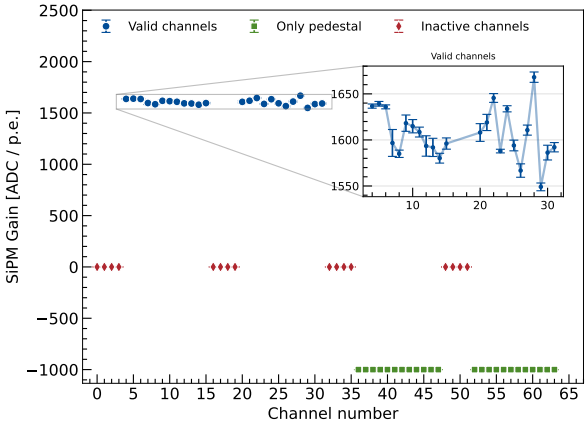

Figure 20. SiPM Gain obtained from the linear interpolation as a function of the channel number.

From the LRS cabling scheme (see Figure 21) we can search for the connections between modules and ADC channels. If we know a priori the LED we are triggering on, we can check that the resulting spectra and consequently SiPM gains are consistent with what we expect. In this specific case the LED A1 was used so we expect ACL 101 and ACL 102, being closer to the source, to have the highest light yield.

On top of this, we can then perform a more detailed analysis. Considering Figure 22, the plot on the left-hand side shows only the channels with a gain greater than 0, divided according to the corresponding LRS module. On the right-hand side we reported the number of PE peaks found for each channel. We find that ACL 101 and ACL 102 show a larger amount of PE peaks, hence a greater light yield: this is in agreement with the expectations.
A key point to keep in mind is that for a fixed gain LCM modules gave a higher light yield than ACL ones. In each run the VGA gain and the LED amplitude are adjusted in order to be optimal for one of the two systems. In principle it might be needed to define different fit ranges and/or parameters to better optimize the script. Nevertheless, for the purpose of quick QA/QC tests the tool was used on a several data-sets (both for LCM and ACL) and it already gives proper results.

[7] For a 10k events sample, the processing time for all 64 channels is less than 10 seconds, making it ideal for quick tests.

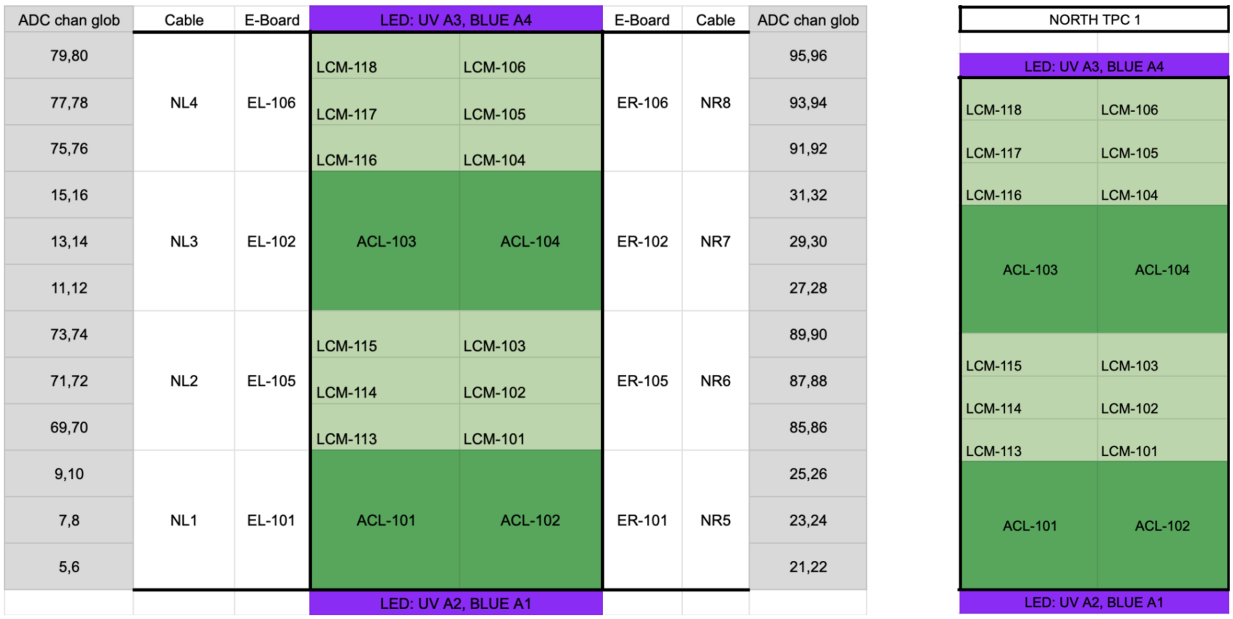

Figure 21. LEFT: Example of LRS cabling scheme: cabling connections between ADC channels and LRS modules are indicated (for one TPC). RIGHT: Zoom on the light modules.

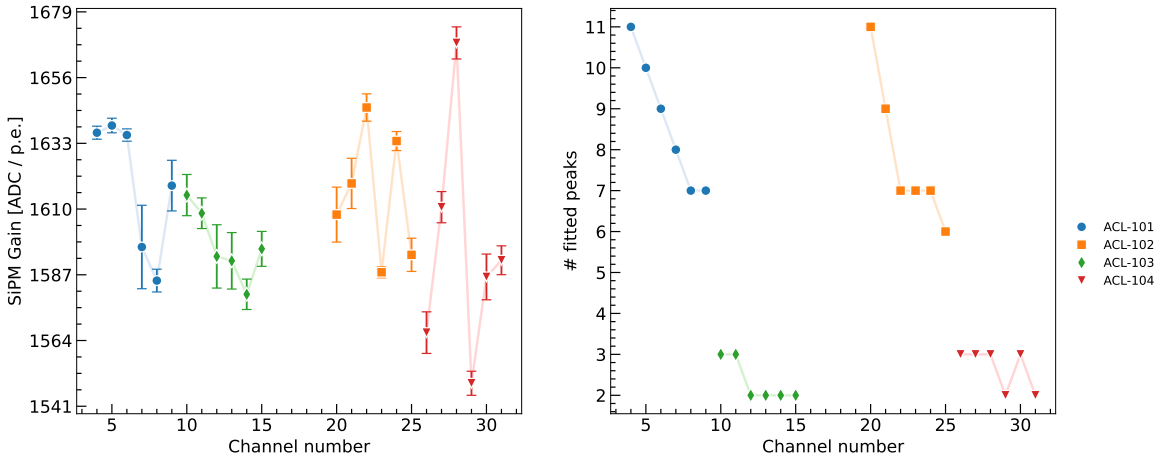

Figure 22. LEFT: SiPM gain as a function of channel number. RIGHT: found PE peaks as a function of channel number. ArClight modules 101 and 102 show the highest number of peaks, hence they have a greater light yield.

Another analysis that can be performed involves the pedestal peak, namely the one due to the noise. From the data files, we can retrieve both its mean value and its standard deviation, and this is automatically done. We expect the mean value to be roughly compatible for all channels, so outliers might highlight a potential issue. The width of the noise peak probably carries more important information: indeed when this value is not in the expected range (for example channels 20 and 55 on the right panel of Figure 23), it may indicate the need to thoroughly checking those specific channels. This part is still under study and it is yet to be defined whether these parameters can be used as good indicators for data quality monitoring.

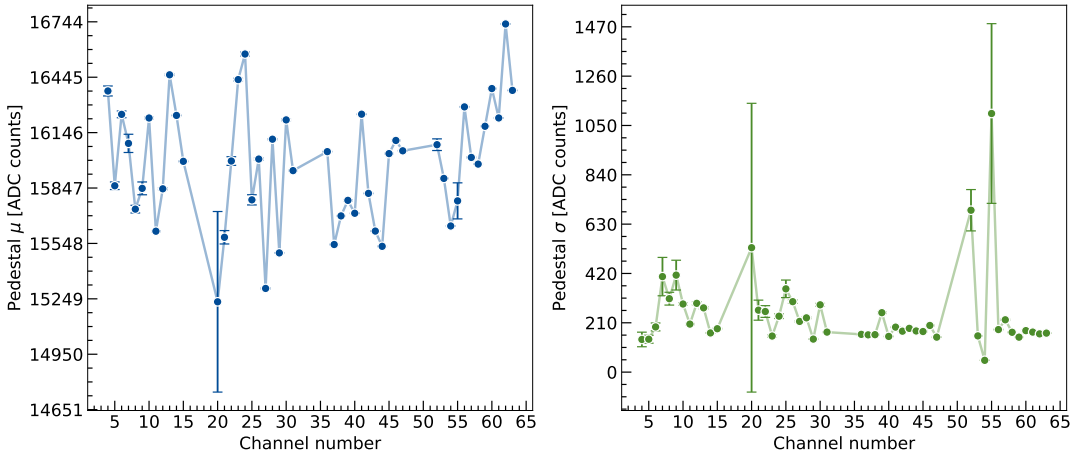

Figure 23. Pedestal mean value (left) and standard deviation (right) as a function of channel number.

7. Conclusions

The main activities I carried out during the internship can be divided into two parts:

1. The first part was related to the Ground Impedance Monitor, installed at LArTF, to ensure the low noise operations of the 2x2 Demonstrator modules. My work was focused on developing a procedure to monitor in real-time the impedance between the detector and the building grounds. Within this context data was saved on a database and then uploaded on an online software.

2. In the second part I was involved in the QA/QC tests of the Argoncube light readout system. I learned and performed the different steps to validate the LRS functionality after transportation and to determine the overall LRS electronics response and performance. Furthermore, my task was focused on developing a tool to analyse the LED calibration run data during the tests. For this purpose, I wrote several scripts to quickly and automatically perform the analysis: the final goal is to compute all SiPMs gain and to find potential malfunctioning channels.

References

[1] Abi Babak et al. Deep Underground Neutrino Experiment (DUNE), Far Detector Technical Design Report, Volume II DUNE Physics. Technical report, Feb 2020. URL https://cds.cern.ch/record/2709273.

[2] ARGONCUBE collaboration website. URL https://argoncube.org.

[3] A. Abed Abud et al. Deep Underground Neutrino Experiment (DUNE) Near Detector Conceptual Design Report. *Instruments*, 5(4), 2021. URL https://www.mdpi.com/2410-390X/5/4/31.

[4] C. Amsler et al. ArgonCube: a novel, fully-modular approach for the realization of large-mass liquid argon TPC neutrino detectors. Technical report, CERN, Geneva, 2015. URL https://cds.cern.ch/record/1993255.

[5] Carlo Rubbia. The liquid-argon time projection chamber: a new concept for neutrino detectors. Technical report, CERN, Geneva, 1977. URL https://cds.cern.ch/record/117852.

[6] A. Ereditato and A. Rubbia. The liquid argon TPC: a powerful detector for future neutrino experiments and proton decay searches. *Nuclear Physics B - Proceedings Supplements*, 154(1):163–178, apr 2006.

[7] José Maneira. Techniques for TPC Calibration: Application to Liquid Ar-TPCs. *Particles*, 5(1):74–83, 2022. doi: 10.3390/particles5010007. URL https://www.mdpi.com/2571-712X/5/1/7.

[8] Roman Matthias Berner. *ArgonCube – A Novel Concept for Liquid Argon Time Projection Chambers.* PhD thesis, Universität Bern, Bern, 2021.

[9] Patrick Koller. *A Method to Improve the Neutrino Energy Reconstruction in LArTPCs.* PhD thesis, Universität Bern, Bern, 2021.

[10] B. Aimard et al. Study of scintillation light collection, production and propagation in a 4 tonne dual-phase LArTPC. *Journal of Instrumentation*, 16(03):P03007, mar 2021. URL https://doi.org/10.1088/1748-0221/16/03/p03007.

[11] J. Asaadi et al. First Demonstration of a Pixelated Charge Readout for Single-Phase Liquid Argon Time Projection Chambers. *Instruments*, 4(1), 2020. URL https://www.mdpi.com/2410-390X/4/1/9.

[12] M. Auger et al. ArCLight—A Compact Dielectric Large-Area Photon Detector. *Instruments*, 2(1), 2018. URL https://www.mdpi.com/2410-390X/2/1/3.

[13] J. Sinclair et al. ProtoDUNE-ND: proposal to place the ArgonCube 2x2 Demonstrator on-axis in NuMI, 2019. URL https://docs.dunescience.org/cgi-bin/private/ShowDocument?docid=12571. DUNE-doc-12571.

[14] A. Ereditato et al. Design and operation of ARGONTUBE: a 5 m long drift liquid argon TPC. *Journal of Instrumentation*, 8(07):P07002–P07002, jul 2013. URL https://doi.org/10.1088/1748-0221/8/07/p07002.

[15] L. Bagby. LArTF Impedance Monitor System for 2x2, 2021. DUNE-doc-25365.

[16] M. Utes P. Rubinov and L. Bagby. Ground Impedance Monitor Installation and Operational Procedures ICARUS Edition, 2021. Engineering Note: EED190530.

[17] John Shahid. Influxdb documentation, 2021. URL https://buildmedia.readthedocs.org/media/pdf/influxdb-python/latest/influxdb-python.pdf.

[18] Grafana labs. Grafana documentation, 2022. URL https://grafana.com/docs/grafana/latest/.

[19] N. Anfimov et al. Development of the light collection module for the liquid argon time projection chamber (LArTPC). *Journal of Instrumentation*, 15(07):C07022–C07022, jul 2020. URL https://doi.org/10.1088/1748-0221/15/07/c07022.

[20] Marcin Kuźniak and Andrzej M. Szelc. Wavelength shifters for applications in liquid argon detectors. *Instruments*, 5(1), 2021. URL https://www.mdpi.com/2410-390X/5/1/4.

[21] Rene Brun and Fons Rademakers. ROOT - An Object Oriented Data Analysis Framework. *Nucl. Inst. & Meth. in Phys. Res. A*, (389):81–86, 1996. Proceedings AIHENP'96 Workshop, Lausanne, Sep. 1996.

8. Appendices

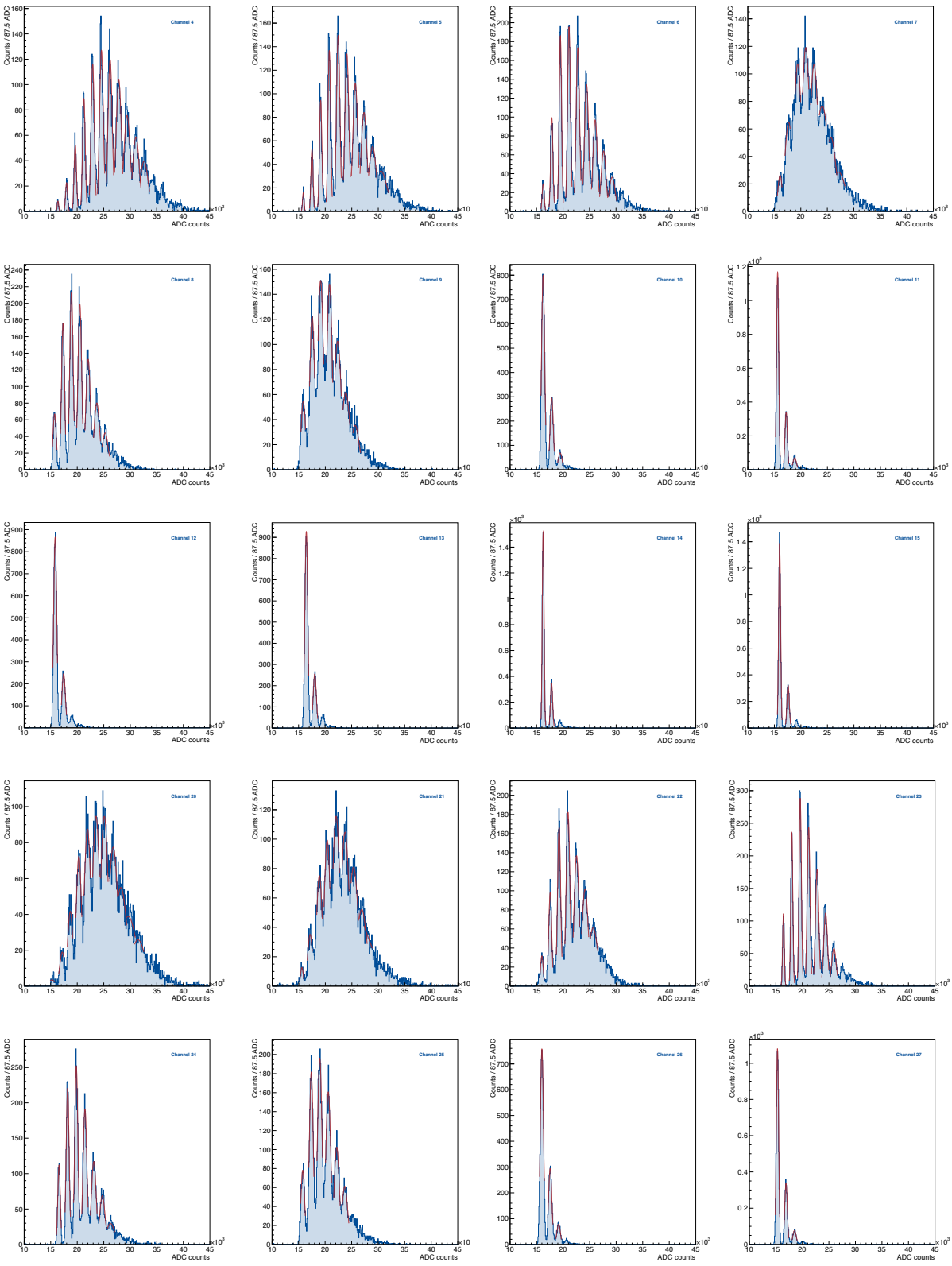

Figure 24. Example of charge spectra for ACL modules. (1)

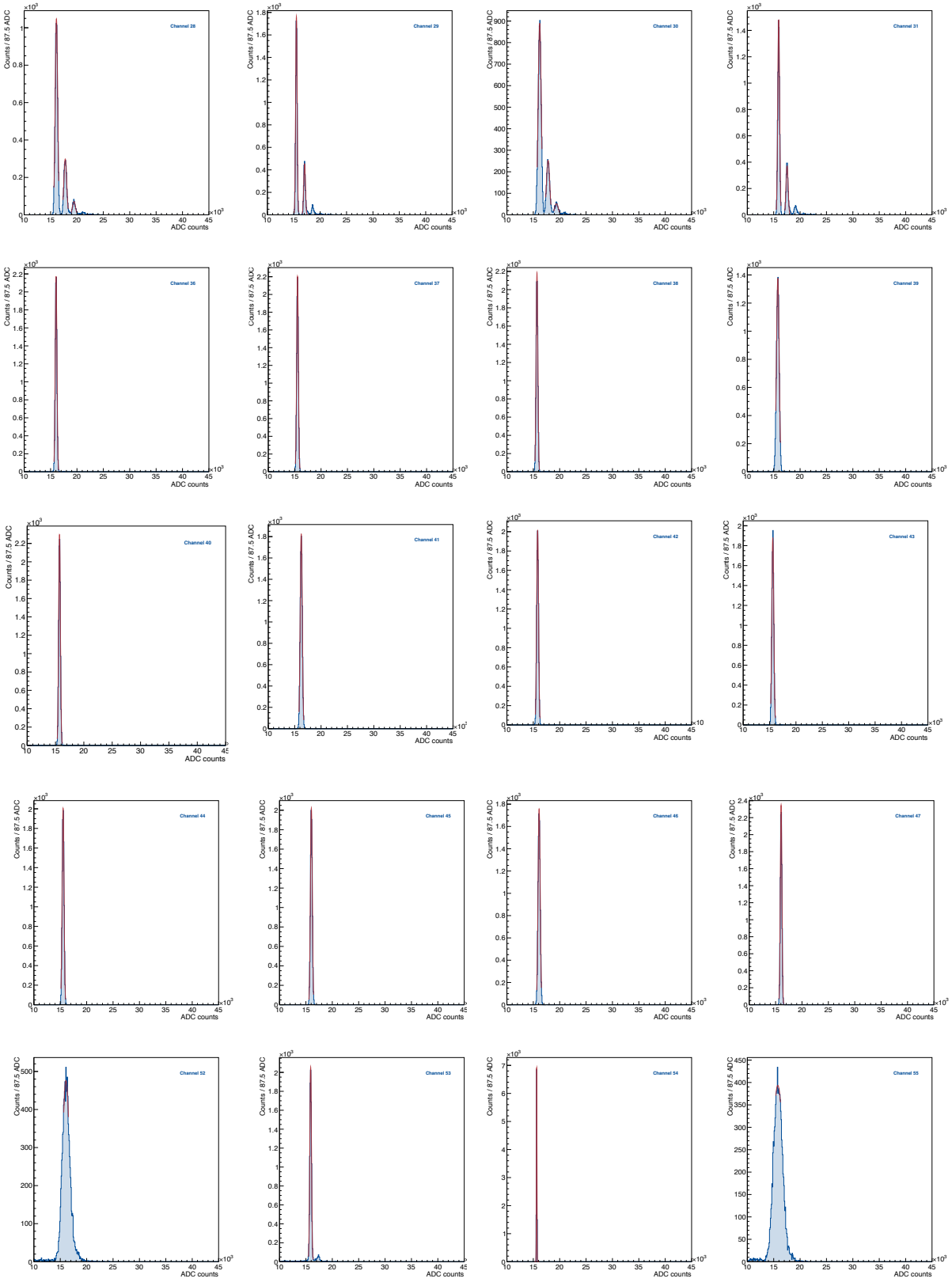

Figure 25. Example of charge spectra for ACL modules. (2)

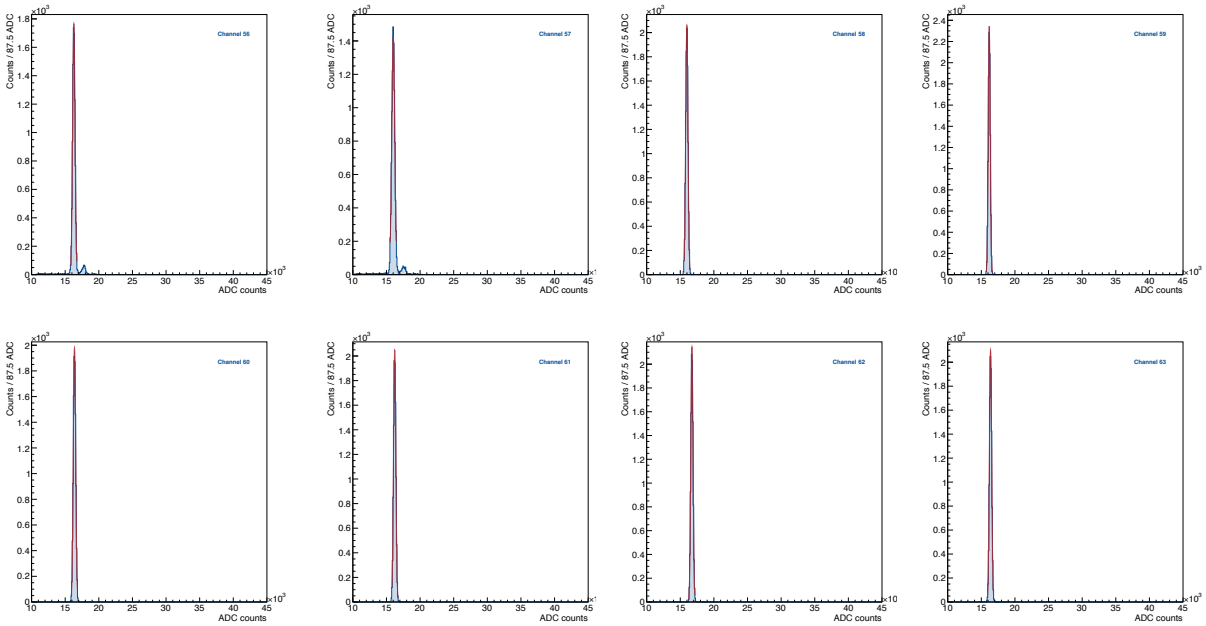

Figure 26. Example of charge spectra for ACL modules. (3)